

Elastic scattering and breakup of ^{17}F at 10 MeV/nucleon

J. F. Liang¹, J. R. Beene¹, H. Esbensen², A. Galindo-Uribarri¹, J. Gomez del Campo¹,
C. J. Gross^{1,3}, M. L. Halbert¹, P. E. Mueller¹, D. Shapira¹, D. W. Stracener¹,
I. J. Thompson⁴ and R. L. Varner¹

¹*Physics Division, Oak Ridge National Laboratory, Oak Ridge, TN 37831, USA*

²*Physics Division, Argonne National Laboratory, Argonne, IL 60439, USA*

³*Oak Ridge Institute for Science and Education, Oak Ridge, TN 37831, USA*

⁴*Department of Physics, University of Surrey, Guildford GU2 5XH, United Kingdom*

(October 31, 2018)

Abstract

Angular distributions of fluorine and oxygen produced from 170 MeV ^{17}F incident on ^{208}Pb were measured. The elastic scattering data are in good agreement with optical model calculations using a double-folding potential and parameters similar to those obtained from $^{16}\text{O}+^{208}\text{Pb}$. A large yield of oxygen was observed near $\theta_{\text{lab}} = 36^\circ$. It is reproduced fairly well by a calculation of the $(^{17}\text{F}, ^{16}\text{O})$ breakup, which is dominated by one-proton stripping reactions. The discrepancy between our previous coincidence measurement and theoretical predictions was resolved by including core absorption in the present calculation.

PACS number(s): 25.60.-t, 25.60.Bx, 25.60.Gc, 25.70.-z

Our knowledge of atomic nuclei comes from experiments with nuclei in the valley of stability. The advent of radioactive beams enables us to explore nuclei near and beyond the drip lines and provides tests of current nuclear structure models. Nuclear reactions are often used as tools for studying nuclear structure. Breakup is an important reaction channel in the scattering of weakly bound nuclei and can be a rich source of information on reaction mechanisms and the structure of such nuclei [1–4].

Fluorine-17 is a proton drip-line nucleus with its valence proton bound by 0.6 MeV. Because of this loose binding, the r.m.s. radius, 3.7 fm [5], is significantly larger than that of the ^{16}O core. Furthermore, the first excited state of ^{17}F , $E_x = 0.495$ MeV and $J^\pi = \frac{1}{2}^+$, is reported to have an extended r.m.s. radius, 5.3 fm [5], and is considered to be a nuclear halo state. Studies of the influence on fusion of breakup of weakly bound nuclei has generated considerable interest in recent years [6]. The measurement of fusion of ^{17}F on ^{208}Pb at energies near the Coulomb barrier found no fusion enhancement [7]. In our previous measurement of the breakup of ^{17}F by detecting the breakup products, proton and ^{16}O , simultaneously, a very small cross section was observed and disagreed with theoretical predictions [8]. That experiment used a large area detector to optimize the collection efficiency; the measured cross sections were averaged over the angles spanned by the detector.

A recent study of the breakup reaction $^8\text{B} \rightarrow ^7\text{Be} + \text{p}$ on a ^{58}Ni target at sub-Coulomb energies [9] demonstrated that the resulting ^7Be angular distribution can be accounted for by two different theoretical approaches, coupled discretized-continuum channels (CDCC) [10] and dynamical calculation [11]. With this in mind, we have performed a new experiment on the breakup of ^{17}F by measuring the angular distribution of reaction products in singles. The data provide some details of the cross section over a range of angles and no Monte Carlo simulation is required for obtaining the efficiency of the detectors, unlike the coincidence measurement. However, the identification of reaction products with the breakup channel is not as straightforward as in the coincidence measurement, since similar products can be produced in several reaction channels. With the aid of theoretical calculations, the dominant reaction products were shown to originate from breakup.

The experiment was carried out at the Holifield Radioactive Ion Beam Facility (HRIBF) using a 170 MeV ^{17}F beam incident on a 2 mg/cm^2 ^{208}Pb target. A 44 MeV deuteron beam provided by the Oak Ridge Isochronous Cyclotron (ORIC) was used to bombard a fibrous hafnium oxide target to produce radioactive ^{17}F by the $^{16}\text{O}(\text{d},\text{n})$ reaction [12]. The $A=17$ ions were extracted from the target-ion source, mass analyzed and subsequently accelerated by the 25 MV tandem postaccelerator. The ^{17}O isobar contaminant was removed by inserting a carbon stripper foil at the exit of the tandem accelerator, before the 90° analyzing magnet, and selecting the fully stripped $^{17}\text{F}^{9+}$ ion beam. The beam was monitored by a Si surface barrier detector positioned at 10° to the beam direction in the target chamber as well as by the focal plane detector in the Enge spectrograph at 3° on the other side of the beam. The average beam intensity was 5×10^5 $^{17}\text{F}/\text{s}$. The reaction products were detected at $\theta_{\text{lab}} = 45^\circ$ by a $\Delta\text{E-E}$ telescope consisting of a large area (900 mm^2) $100 \mu\text{m}$ Si surface barrier detector (SBD) and a $5 \text{ cm} \times 5 \text{ cm}$, $300 \mu\text{m}$ double-sided Si strip detector (DSSD) behind the SBD. The DSSD, which has 16 vertical and 16 horizontal strips, was placed 8.3 cm from the target, resulting in an angular resolution of $\sim 2^\circ$. At forward angles, the elastically scattered ^{17}F was measured by the DSSD only.

Figure 1 shows the E vs. ΔE histogram of the SBD-DSSD telescope for events in all the strips. Reaction products of Z=9(F), 8(O), 7(N), 6(C), 5(B) and 1(H) were observed. The band of constant energy loss (ΔE) at channel number ~ 135 , corresponding to the energy loss of the elastically scattered ^{17}F , results from the positron decay of ^{17}F stopped in the DSSD. These events were recorded when a positron emission took place at the same time as an elastic ^{17}F struck another strip in the DSSD.

The elastic scattering data were extracted from the Z=9 products identified in this E vs. ΔE histogram. The energy resolution of the detectors was not good enough to allow a clear separation between the elastic and inelastic scattering events. Moreover, the mass of the reaction products cannot be identified in this experiment. Since there are some neutron pickup channels with positive Q values, the elastic scattering data may include contributions from inelastic scattering and neutron transfer reactions. The absolute cross section was obtained by normalizing the yields to the Si detector at 10° where the elastic scattering was taken as Rutherford scattering. The elastic scattering angular distribution is shown in Fig. 2. As can be seen, the assumption of pure Rutherford scattering at 10° is valid.

Optical model fits to the elastic scattering data were performed using the code *Ptolemy* [13]. The Woods-Saxon potential parameters were taken from the 192 MeV $^{16}\text{O} + ^{208}\text{Pb}$ elastic scattering [14] and only the depth of the imaginary potential was allowed to vary. The best-fit result is shown by the dotted curve in Fig. 2 and the parameters are listed in Table I as SET I. Parameters in SET II of Table I were obtained using the procedures described in Ref. [14] by fitting the data with the depth of the real potential, V, fixed at 40 MeV and varying the other parameters. Throughout the fitting processes, the shape of the real and imaginary potential was assumed to be the same. The imaginary potential depth, W, was changed from 35 to 95 MeV in 5 MeV steps and the radius and diffuseness parameters, r and a, were varied to find the minimum χ^2 . The best fit is shown by the dash-dotted curve. The radius and diffuseness parameters were very similar to those obtained in the 140 MeV $^{16}\text{O} + ^{208}\text{Pb}$ elastic scattering [15]. The dashed curve, corresponding to parameter SET III, is the result of allowing all the parameters, V, W, r, and a, to vary subject to the constraint that r and a were identical for the real and imaginary potentials. The dashed curve and dash-dotted curve are almost indistinguishable. All three sets of parameters describe the data very well at angles smaller than 41° . However, differences between the dotted curve and dashed curve can be seen at larger angles. The inclusion of inelastic scattering and transfer in the data may account for the fact that the experimental points are above the dotted prediction.

The elastic scattering data were also compared to calculations using potentials obtained from a double-folding model. The effective nucleon-nucleon interaction was taken from Satchler's systematics [16] which uses the three-parameter Yukawa form

$$U_{\text{NN}} = -(V + iW) \frac{e^{-s/t}}{s/t}$$

where s is the distance between the two nucleons and $t = 0.7$ fm. The depth of the potentials was $V = W = 60 - 0.3E/A = 57$ MeV where E/A is the energy per nucleon of the projectile. The nuclear density distribution of ^{208}Pb was constructed using the two-parameter Fermi form with parameters given in Table 2 of Ref. [16]. The ground state density distribution

of ^{17}F was constructed from shell model single particle wave functions as described by Satchler [17] (method B). Calculations using this double-folding potential with no adjustable parameters are in very good agreement with the data, as shown by the solid curve in Fig. 3. Beyond about 45° , the calculation underpredicts the data somewhat, which may be due to the inclusion of inelastic scattering and neutron transfer reactions in the data. The inelastic excitation of ^{17}F to its first excited state, $E_x = 0.495$ MeV and $J^\pi = \frac{1}{2}^+$, and ^{208}Pb to its first 2^+ , $E_x = 4.09$ MeV, and 3^- , $E_x = 2.61$ MeV, states were calculated in the DWBA by the code `Ptolemy`. The sum of the inelastic scattering predicted by DWBA and the elastic scattering predicted by the folding potential is shown by the dotted curve in Fig. 3 which is in excellent agreement with the data. Among the three inelastic channels, the excitation cross section for populating the first excited state of ^{17}F is calculated to be the largest, followed by exciting ^{208}Pb to its first 3^- state. Since the single particle wave function used seems to give a good account of the ground state density distribution of ^{17}F , the halo property of the first excited state in ^{17}F could be studied if the inelastic scattering could be resolved in the data. Coupled-channels calculations were performed with these three inelastic channels using `Ptolemy`. As can be seen by the dashed curve in Fig. 3, the elastic scattering is influenced only slightly by the channel couplings. The one-neutron transfer reaction was calculated by DWBA using `Ptolemy`. The transfer yield was predicted to be at least two orders of magnitude less than the elastic scattering and can be ignored, consistent with the agreement between the data and the dotted curve in Fig. 3.

The angular distribution of $Z=8$ reaction products used the same normalization as the elastic scattering. Since this experiment provided no mass identification of the reaction products, the observed oxygen can originate from nucleon transfer, charge exchange, and breakup. The one-proton transfer has the largest Q value of all transfer channels leading to an oxygen isotope, ^{16}O , as the final product. Finite range DWBA calculations using the code `Ptolemy` were performed to predict the cross section angular distribution of $^{208}\text{Pb}(^{17}\text{F}, ^{16}\text{O})^{209}\text{Bi}$. Transfer to the lowest six single particle states in ^{209}Bi was calculated. The spectroscopic factors were assumed to be 1 which will give upper limits for the cross sections. The sum of the six cross sections is shown by the dotted curve in Fig. 4. It can be seen that the one-proton transfer cannot account for the yields of the oxygen angular distribution. Similar results were obtained for calculations using the code `FRESCO` [18]. Although reactions leading to ^{18}O and ^{207}Bi in the exit channel have positive Q values, they cannot occur by simple single-step transfer processes. Therefore, the cross sections are expected to be smaller than that of one-proton transfer [19].

Oxygen-17 can be produced by the charge exchange reaction, $^{208}\text{Pb}(^{17}\text{F}, ^{17}\text{O})^{208}\text{Bi}$, with a Q value of -0.11 MeV. Calculations were performed to estimate the cross section for this reaction channel. Charge exchange reactions can take place by direct charge exchange, a combination of inelastic excitation and direct charge exchange, or by successive one-nucleon exchange. Since the direct charge exchange is orders of magnitude smaller than one-nucleon transfer [20], calculations were carried out using `FRESCO` to model the successive one-nucleon exchange processes [21]. Two possible modes, proton stripping followed by neutron pickup and neutron pickup followed by proton stripping, were considered. Only transfer between ground states was calculated. The charge exchange cross section is calculated to be 2 orders of magnitude smaller than that of one-proton transfer calculated by DWBA. Measurements of $^{28}\text{Si}(^{18}\text{O}, ^{18}\text{F})^{28}\text{Al}$ show that the charge exchange cross section is at least an order of

magnitude smaller than that of one-nucleon transfer [22], consistent with the results of our calculations. Since DWBA calculations predict that the one-proton transfer cross sections are much smaller than the measured cross sections, it is safe to assume that charge exchange can be ignored.

The measurement is inclusive, so products from two breakup processes, diffraction and stripping, can contribute to the data [2]. In diffraction dissociation, the projectile breaks up, leaving the valence nucleon in the continuum and the core intact. The final state of the reaction consists of the valence nucleon, the core of the projectile and the target nucleus in its ground state. This is the process that our previous coincidence experiment measured [8]. The stripping breakup depends on the core-target and nucleon-target absorption potentials. In a loosely bound nuclear system, if the separation energy (S_N) is much less than the kinetic energy per nucleon, $S_N \ll E/A$, the valence nucleon and the core can be treated approximately as independent particles [23]. The effects of nucleon-target and core-target interactions become noticeable if the interactions are strong.

Semiclassical calculations of breakup similar to those in Ref. [2] were performed to investigate these processes. The wave function of the projectile after interacting with the target is described by the ground state wave function of the projectile and the profile functions of the proton and ^{16}O core. The interaction between the target nucleus and the constituents of the projectile was obtained from Ref. [24]. The ^{16}O -target optical potential was calculated in a single-folding model based on the CH89 optical model potential [24]. The breakup probability as a function of the impact parameter was calculated and converted to an angular distribution assuming pure Coulomb scattering. The calculated angular distribution was converted from the center of mass of the reaction to the laboratory frame using the Jacobian for elastic scattering. Because the reaction energy is high, the uncertainty introduced by this approximation is smaller than the angular resolution of the DSSD.

Figure 4 presents the comparison of the experimental oxygen cross section data with model calculations. The long-dashed curve is the prediction for stripping breakup while the short-dashed curve is for diffraction breakup. Apparently, stripping breakup is the dominant reaction in the measured angular range. The solid curve shows the sum of diffraction and stripping. It overpredicts the measured cross sections slightly; however, the data do not extend far enough forward for a good comparison. It should be pointed out that the calculations employed here did not consider the recoil of the ^{16}O . In addition, excitation of the ^{16}O and ^{208}Pb in the final state was ignored. Measurements of the breakup of ^{17}C by ^{197}Au show that core excitation is important for nuclear breakup [25], but very small for Coulomb breakup [26]. In our case, the measurement was performed near the grazing angle where the nuclear breakup should be significant. Therefore, the excitation of the core and target nuclei should be considered. Furthermore, the stripping and diffraction breakup were calculated separately. A more complete theoretical treatment of this subject is underway and will be published elsewhere [27].

Diffraction breakup of ^{17}F was measured previously in our coincidence experiment [8]. A first-order perturbation calculation overpredicted the measured cross section by a factor of 4. The present work shows the importance of stripping breakup resulting from the nucleon-target interaction. The discrepancy in the coincidence experiment can be accounted for by including the core absorption by the target nucleus which was not considered in the previous calculations. As shown in Fig. 5, the data agree with the calculations taking into account

the core-target interaction (short-dashed curve). The calculation is also consistent with predictions made by the CDCC calculation [10] shown by the dash-dotted curve. The CDCC calculation takes into account of higher order effects, continuum-continuum couplings, and full three-body kinematics to produce results in the laboratory frame [28].

It is shown in Ref. [2] that the breakup of ^{11}Be ($S_N = 0.5$ MeV) by ^{208}Pb is dominated by stripping at 800 MeV/nucleon. At 40 MeV/nucleon, the stripping and diffraction breakup cross sections become similar [2]. In the breakup of ^8B at energies below the Coulomb barrier, the stripping and diffraction breakup cross sections are also similar [9]. In this work, it is found that the stripping breakup cross section of 10 MeV/nucleon ^{17}F is almost twice as large as that of the diffraction breakup.

In summary, the elastic scattering and breakup of ^{17}F was measured on a ^{208}Pb target. The elastic scattering data were fitted with an optical model using a Woods-Saxon potential. The potential parameters are very similar to those obtained from $^{16}\text{O}+^{208}\text{Pb}$ elastic scattering. The potential generated from a double-folding model using Satchler's systematics also reproduced the elastic scattering data. The dominant contribution to the measured angular distribution of oxygen nuclei in the exit channel was found to be the one-proton stripping reaction resulting in ^{16}O . This demonstrates the importance of the proton-target interaction in the breakup of ^{17}F on ^{208}Pb . Based on this finding, calculations of diffraction breakup considering core absorption were carried out. The new calculations agree with our previous coincidence measurement.

We would like to thank J. B. Ball, D. J. Dean, J. J. Kolata, F. M. Nunes, G. R. Satchler, and C. Y. Wong for informative discussions. We are specially grateful to N. Keeley for the charge exchange calculations. The experimental measurements would not have been possible without the hard work of the HRIBF staff. Research at the Oak Ridge National Laboratory is supported by the U.S. Department of Energy under contract DE-AC05-00OR22725 with UT-Battelle, LLC. The ORISE is supported by the U.S. Department of Energy under contract number DE-AC05-00OR22750. One of us (H.E.) was supported by the U.S. Department of Energy, Nuclear Physics Division, under Contract No. W-31-109-ENG-38.

REFERENCES

- [1] R. Anne *et al.*, Phys. Lett. B **304**, 55 (1993).
- [2] K. Hencken, G. F. Bertsch, and H. Esbensen, Phys. Rev. C **54**, 3043 (1996).
- [3] F. Barranco, E. Vigezzi, and R. A. Broglia, Z. Phys. A **356**, 45 (1996).
- [4] A. Navin *et al.*, Phys. Rev. Lett. **81**, 5089 (1998).
- [5] R. Morlock *et al.*, Phys. Rev. Lett. **79**, 3837 (1997).
- [6] C. Signorini, J. Phys. G **23**, 1235 (1997), and references therein.
- [7] K. E. Rehm *et al.*, Phys. Rev. Lett. **81**, 3341 (1998).
- [8] J. F. Liang *et al.*, Phys. Lett. B **491**, 23 (2000).
- [9] V. Guimarães *et al.*, Phys. Rev. Lett. **84**, 1862 (2000).
- [10] F. M. Nunes and I. J. Thompson, Phys. Rev. C **59**, 2652 (1999).
- [11] H. Esbensen and G. F. Bertsch, Phys. Rev. C **59**, 3240 (1999).
- [12] R. F. Welton *et al.*, Nucl. Instrum. Methods B **159**, 116 (1999).
- [13] M. H. Macfarlane and S. C. Pieper, Report No. ANL-76-11 Rev. 1, 1978 (unpublished).
- [14] J. B. Ball *et al.*, Nucl. Phys. **A252**, 208 (1975).
- [15] D. G. Kovar *et al.*, Phys. Rev. Lett. **30**, 1075 (1973).
- [16] G. R. Satchler, Nucl. Phys. **A579**, 241 (1994).
- [17] G. R. Satchler, Nucl. Phys. **A329**, 233 (1979).
- [18] I. J. Thompson, Comput. Phys. Rep. **7**, 167 (1988).
- [19] D. G. Kovar in *Proceedings of the International Conference on Reactions between Complex Nuclei*, edited by R. C. Robinson, F. K. McGowan, J. B. Ball, J. H. Hamilton (North-Holland-American Elsevier 1974).
- [20] H. H. Duhm *et al.*, Phys. Lett. B **48**, 1 (1974).
- [21] N. Keeley, private communication.
- [22] B. T. Kim *et al.*, Phys. Rev. C **20**, 1396 (1979).
- [23] K. Yabana, Y. Ogawa, and Y. Suzuki, Nucl. Phys. **A539**, 295 (1992).
- [24] R. L. Varner *et al.*, Phys. Rep. **201**, 57 (1991).
- [25] V. Maddalena and R. Shyam, Phys. Rev. C **63**, 051601(R) (2001).
- [26] R. Shyam and P. Danielewicz, Phys. Rev. C **63**, 054608 (2001).
- [27] H. Esbensen, to be published.
- [28] J. A. Tostevin, F. M. Nunes, and I. J. Thompson, Phys. Rev. C **63**, 024617 (2001).

TABLES

	V (MeV)	W (MeV)	r = r _i (fm)	a = a _i (fm)
SET I	40	49	1.23	0.63
SET II	40	75	1.28	0.50
SET III	50	93	1.27	0.51

TABLE I. Optical model potential parameters obtained from fitting the 170 MeV $^{17}\text{F}+^{208}\text{Pb}$ elastic scattering data. The depth of the real and imaginary potentials is shown by V and W, respectively. The real and imaginary radius parameters are shown by r and r_i, respectively. The real and imaginary diffuseness parameters are shown by a and a_i, respectively.

FIGURES

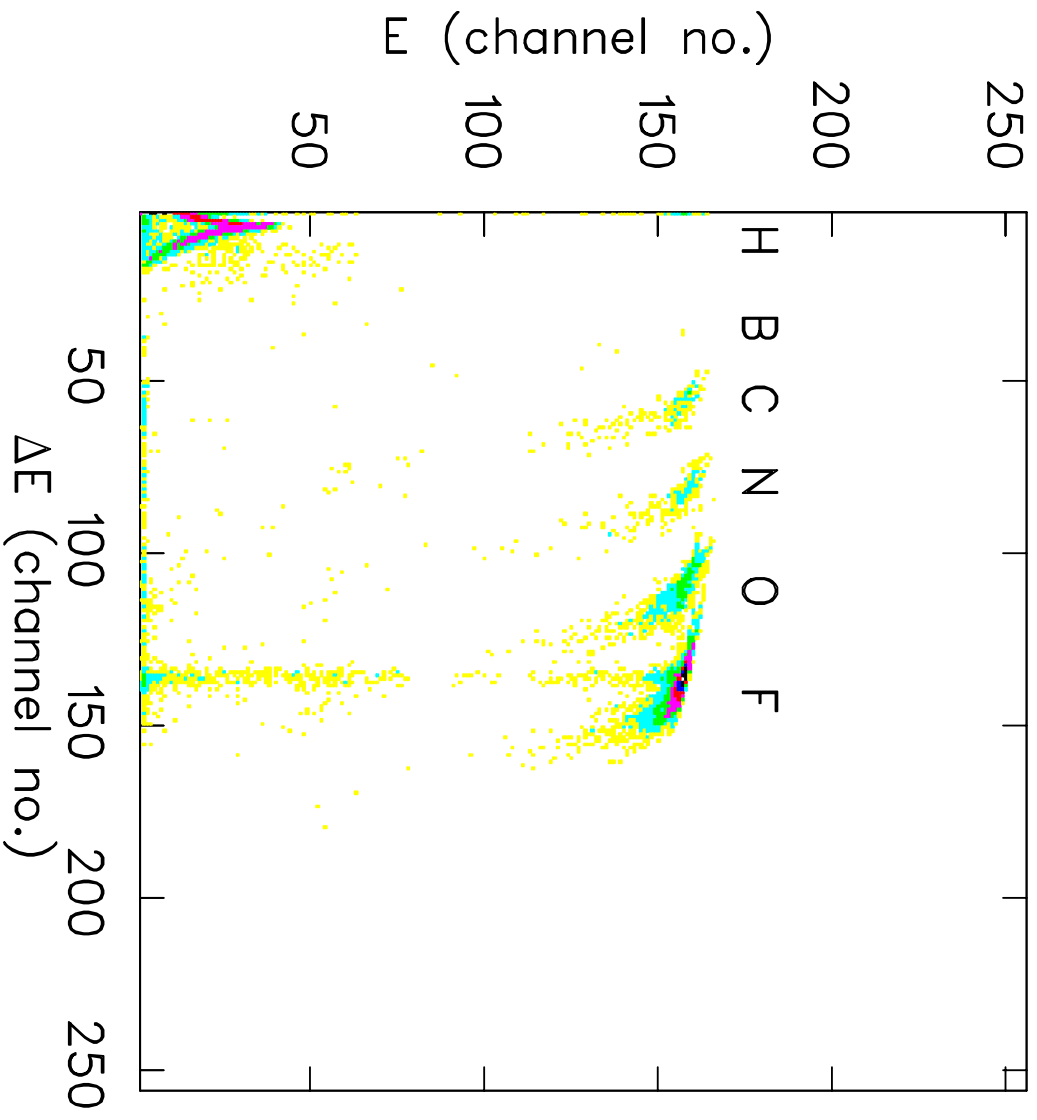
FIG. 1. Histogram of E vs. ΔE obtained by the SBD-DSSD telescope.

FIG. 2. Angular distribution of the ratio of measured elastic scattering to calculated Rutherford scattering. The optical potential fit to the data is shown by the dotted curve for parameters SET I, dash-dotted curve for SET II, and dashed curve for SET III. The dash-dotted curve and dashed curve are almost indistinguishable.

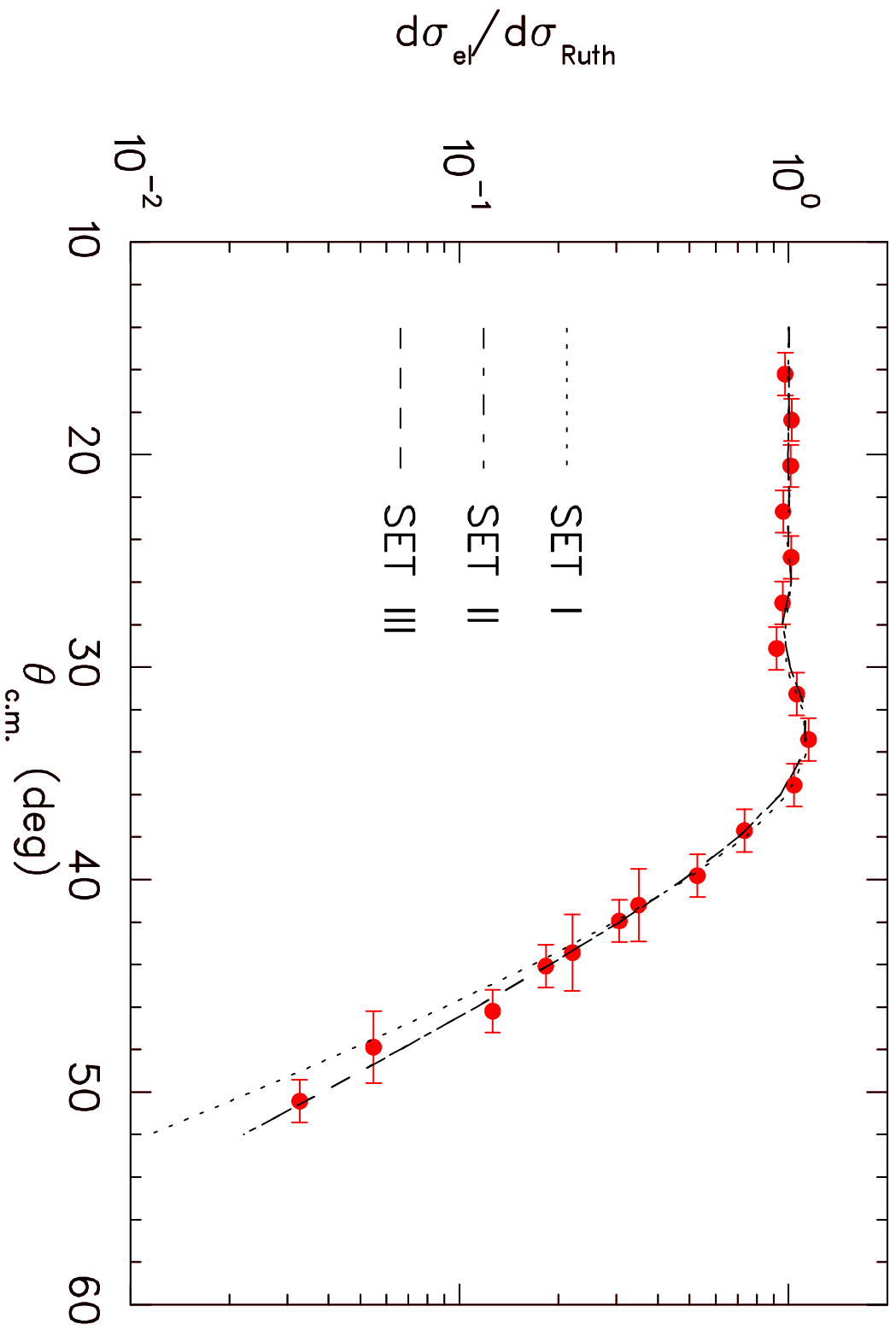
FIG. 3. Angular distribution of the ratio of measured elastic scattering to calculated Rutherford scattering. The solid curve is the result of calculations using the optical potential obtained from a double-folding model. The sum of elastic and inelastic scattering calculations is shown by the dotted curve. The result of coupled-channels calculations is shown by the dashed curve.

FIG. 4. Angular distribution of oxygen. The long-dashed and short-dashed curves are for stripping and diffraction breakup, respectively. The dotted curve is the result of a one-proton transfer DWBA calculation. The solid curve represents the sum of stripping and diffraction breakup.

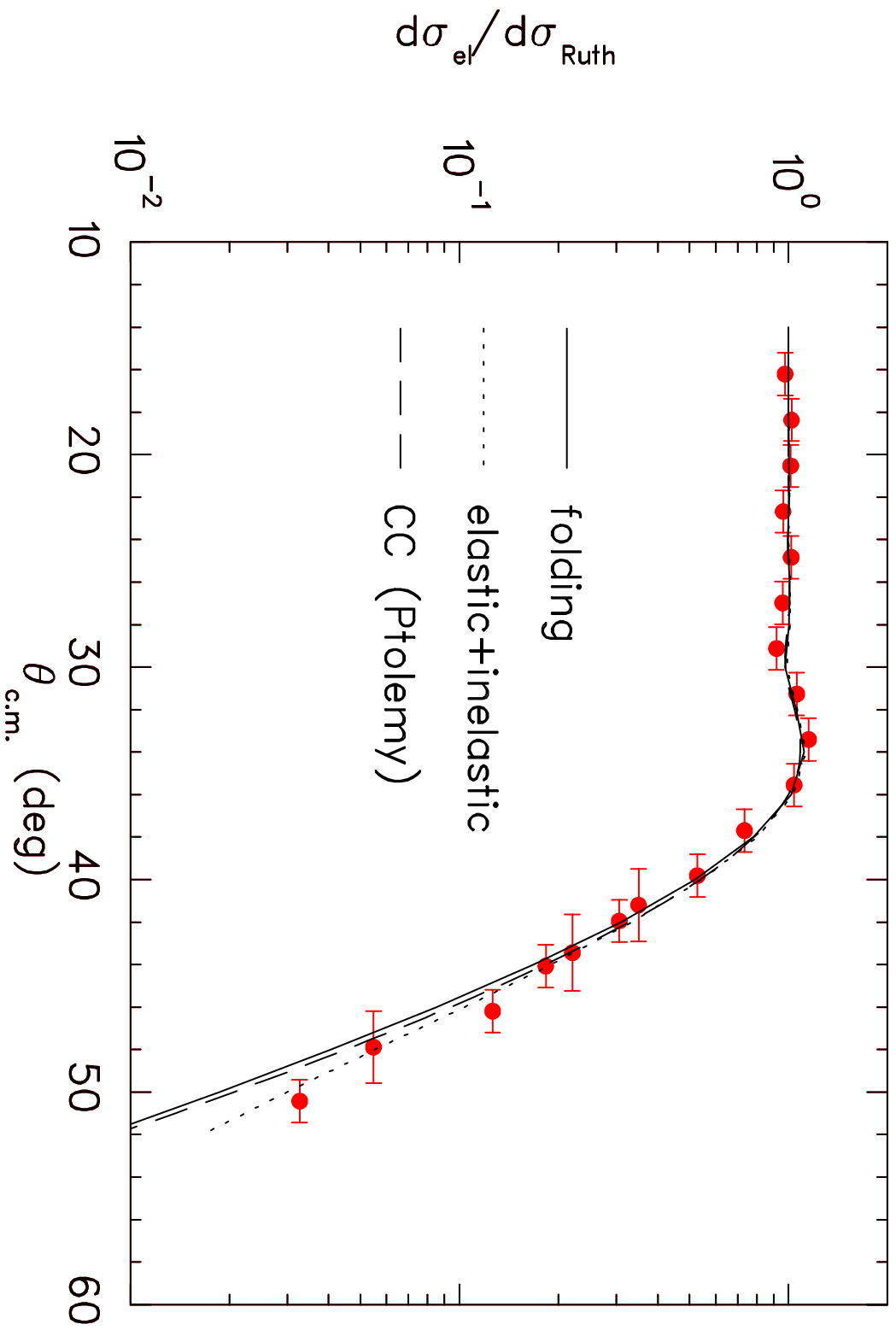
FIG. 5. Data and predictions of diffraction breakup. The long-dashed curve is for the calculation without considering core absorption and the short-dashed curve includes core absorption. The CDCC calculation is shown by the dash-dotted curve. The open point is from our previous measurement [8].



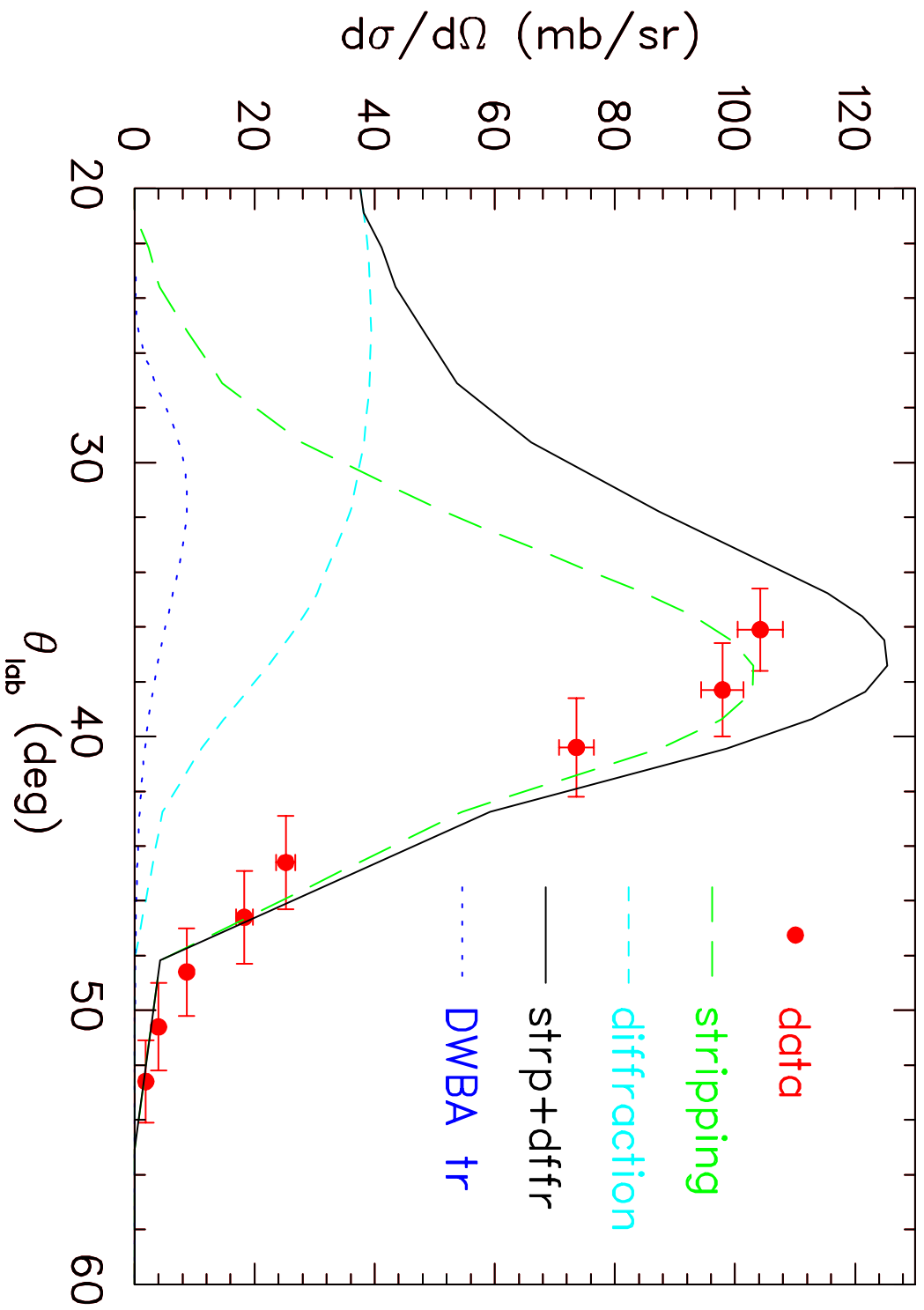
Liang et al. Fig. 1



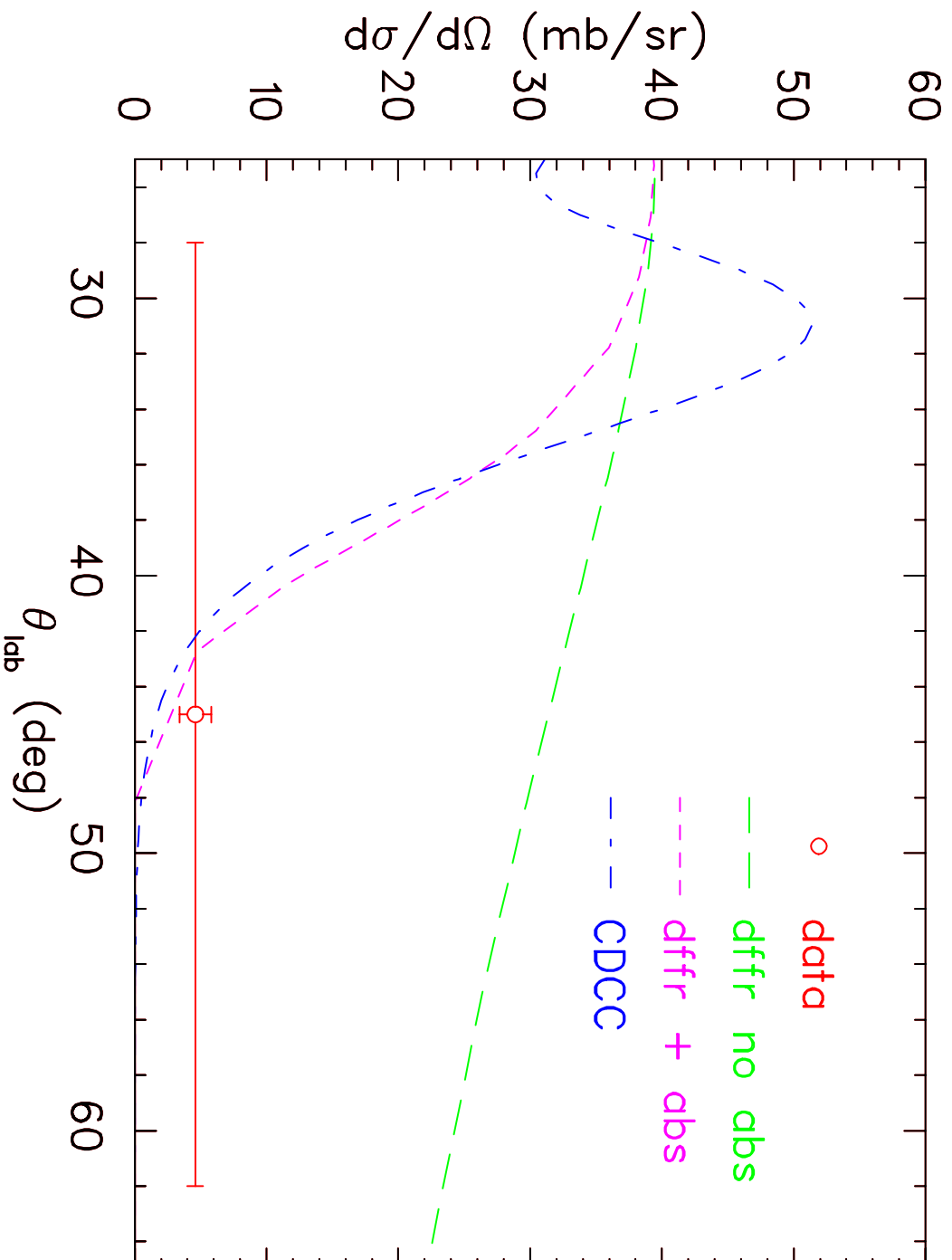
Liang et al. Fig. 2



Liang et al. Fig. 3



Liang et al. Fig. 4



Liang et al. Fig. 5